Molecular Biology of the Cell
Vol. 19, 2949–2961, July 2008

# The Endocytic Adaptor Protein ARH Associates with Motor and Centrosomal Proteins and Is Involved in Centrosome Assembly and Cytokinesis

**Sanna Lehtonen,*† Mehul Shah,*† Rikke Nielsen,* Noriaki Iino,* Jennifer J. Ryan,‡ Huilin Zhou,*‡ and Marilyn G. Farquhar*§**

Departments of *Cellular and Molecular Medicine and §Pathology, and ‡Ludwig Institute for Cancer Research, University of California San Diego, La Jolla, CA 92093

Submitted June 4, 2007; Revised March 27, 2008; Accepted April 9, 2008
Monitoring Editor: Yixian Zheng

**Numerous proteins involved in endocytosis at the plasma membrane have been shown to be present at novel intracellular locations and to have previously unrecognized functions. ARH (autosomal recessive hypercholesterolemia) is an endocytic clathrin-associated adaptor protein that sorts members of the LDL receptor superfamily (LDLR, megalin, LRP). We report here that ARH also associates with centrosomes in several cell types. ARH interacts with centrosomal (γ-tubulin and GPC2 and GPC3) and motor (dynein heavy and intermediate chains) proteins. ARH cofractionates with γ-tubulin on isolated centrosomes, and γ-tubulin and ARH interact on isolated membrane vesicles. During mitosis, ARH sequentially localizes to the nuclear membrane, kinetochores, spindle poles and the midbody. *Arh*$^{-/-}$ embryonic fibroblasts (MEFs) show smaller or absent centrosomes suggesting ARH plays a role in centrosome assembly. Rat-1 fibroblasts depleted of ARH by siRNA and *Arh*$^{-/-}$ MEFs exhibit a slower rate of growth and prolonged cytokinesis. Taken together the data suggest that the defects in centrosome assembly in ARH depleted cells may give rise to cell cycle and mitotic/cytokinesis defects. We propose that ARH participates in centrosomal and mitotic dynamics by interacting with centrosomal proteins. Whether the centrosomal and mitotic functions of ARH are related to its endocytic role remains to be established.**

## INTRODUCTION

The autosomal recessive hypercholesterolemia (ARH) protein is a cargo-specific coat protein that sorts members of the low-density lipoprotein receptor (LDLR) family. It binds to FXNPXY motifs in the cytoplasmic tail of LDLR family members including the LDLR (Garcia *et al.*, 2001; He *et al.*, 2002; Wilund *et al.*, 2002; Cohen *et al.*, 2003), megalin (Nagai *et al.*, 2003) and LDLR-related protein (LRP; Jones *et al.*, 2003) via an N-terminal phosphotyrosine binding (PTB) domain (Garcia *et al.*, 2001; He *et al.*, 2002; Wilund *et al.*, 2002; Cohen *et al.*, 2003). In ARH patients as well as in *Arh*$^{-/-}$ mice, the ARH protein is indispensable for LDL-mediated uptake of LDLR in hepatocytes, lymphocytes, and macrophages, but in other cells (e.g., dermal fibroblasts) another PTB domain protein disabled-2 (Dab-2) substitutes for ARH in facilitating LDL uptake (Garcia *et al.*, 2001; Jones *et al.*, 2003; Keyel *et al.*, 2006; Maurer and Cooper, 2006). ARH also binds to phosphoinositides through its PTB domain and to clathrin and the β subunit of AP-2 via a C-terminal clathrin-box and an AP-2–binding region, respectively (He *et al.*, 2002; Mishra *et al.*, 2002, 2005). Based on these properties, ARH has been designated a clathrin-associated sorting protein (CLASP) that functions in clathrin-mediated endocytosis of receptors of the LDLR superfamily (Brett and Traub, 2006). In addition to its role as a CLASP, the C-terminus of ARH contains a PDZ-interacting motif (PIM) through which ARH can potentially serve as a scaffold protein and interact with and recruit PDZ proteins. Various other cytoplasmic adaptors (e.g., JiP-1, JiP2, Dab-1, ICAP-1) that interact with the cytoplasmic tails of LDLR family members have been shown to mediate diverse cellular functions such as cytoskeletal reorganization, neuronal migration, and vesicle trafficking (Gotthardt *et al.*, 2000).

We reported earlier that ARH binds the FXNPXY motif of the endocytic receptor megalin and accompanies megalin along the endocytic pathway from early endosomes to pericentriolar recycling endosomes located in close proximity to centrosomes (Nagai *et al.*, 2003). Here we report that in addition to its localization to components of the endocytic pathway, ARH is also present at the centrosome at interphase, and during mitosis it localizes sequentially to kinetochores, spindle poles, and the midbody. By mass spectrometry, ARH was also found to interact with components of the γ-tubulin ring complex (γ-TuRC) responsible for microtubule nucleation at the centrosome (Zheng *et al.*, 1995; Schiebel, 2000; Moritz and Agard, 2001) and with components of the cytoplasmic dynein motor machinery. Moreover, cells lacking ARH exhibit defects in centrosome assem-

This article was published online ahead of print in *MBC in Press* (http://www.molbiolcell.org/cgi/doi/10.1091/mbc.E07–05–0521) on April 16, 2008.

† These authors contributed equally to this work.

Address correspondence to: Marilyn G. Farquhar (mfarquhar@ucsd.edu).

Abbreviations used: aa, amino acids; ARH, autosomal recessive hypercholesterolemia; dynein HC, dynein heavy chain; dynein IC, dynein intermediate chain; GCP2/GCP3, gamma-tubulin complex protein 2/3; GST, glutathione *S*-transferase; γ-TURC, γ-tubulin ring complex; IF, immunofluorescence; LDLR, low-density lipoprotein receptor; LRP, LDLR-related protein; MEF, mouse embryo fibroblast; PTB, phosphotyrosine binding; wt, wild type.

bly, prolonged cytokinesis, and a slower growth rate, indicating that the interaction of ARH with these newly identified protein partners is functionally significant.

## MATERIALS AND METHODS

### *Materials*

Chemical reagents and detergents were purchased from Sigma Aldrich (St. Louis, MO) or Fisher Biotech (Tustin, CA). Plasticware for cell culture was purchased from Corning (Corning, NY) and Kodak Biomax MR film from Fisher Biotech.

### *Cell Culture*

L2, rat-1, HeLa cells (obtained from ATTC, Manassas,VA), BAEC, (obtained from Chris Glass, UCSD, La Jolla, CA), and embryonic fibroblasts (MEFs, passages 2–8) from wild-type (wt) and $Arh^{-/-}$ mice (from Dr. Joachim Herz, UT Southwestern, Dallas, TX) were maintained (95% air-5% $CO_2$) in DMEM, high glucose (GIBCO Invitrogen, Grand Island, NY), supplemented with 10% FBS (Hyclone, Logan, UT), 100 U/ml penicillin, 100 $\mu$g/ml streptomycin, and 2 mM glutamine. Mitotic rat-1 cells were enriched using a double-thymidine block (2 mM thymidine for 24 h, 6-h chase in fresh medium, 2 mM thymidine for an additional 18 h, and final 10-h chase). hTERT-RPE cells (from Dr. Stephen Doxsey, University of Massachusetts, Worcester, MA), were cultured in DMEM/F12 (GIBCO), 10% FBS (Hyclone), 7.5 mM HEPES, 100 U/ml penicillin, and 100 $\mu$g/ml streptomycin.

### *Antibodies*

Rabbit anti-ARH 3392 and 3393 were raised against a glutathione S-transferase (GST)-fusion protein (aa 170–299) of rat ARH as described earlier (Nagai *et al.*, 2003). An additional ARH rabbit IgG was kindly provided by Dr. Linton Traub (University of Pittsburgh, Pittsburgh, PA). The other antibodies used in this study were as follows: rabbit dynein HC and mouse MKLP1 IgG (Santa Cruz Biotechnology, Santa Cruz, CA); rabbit histone-H3 and mouse myc IgG (Cell Signaling, Danvers, MA); rabbit phosphohistone-H3 IgG (Upstate Biotechnology, Lake Placid, NY); mouse dynein intermediate chain (IC) IgG (Chemicon International, Temecula, CA); mouse $\gamma$-tubulin, actin, and $\alpha$-tubulin DM1A IgG (Sigma); mouse $p150^{glued}$, dynactin p50, Rab5, and Rab11 IgG (BD Transduction Laboratories, Lexington, KY); mouse syntaxin 13 IgG (StressGen, Ann Arbor, MI); human centromere IgG (Antibodies Incorporated, Davis, CA); rabbit centrin2 IgG (Abcam, Cambridge, MA); rabbit $\gamma$-tubulin complex protein 2 (GCP2) and 3 (GCP3) IgG (Dr. Tim Stearns, Stanford University, CA); human anti-pericentrin (autoimmune) serum 5051 (Dr. Stephen Doxsey, University of Massachusetts, Worcester, MA); HRP-conjugated goat anti-rabbit and anti-mouse IgG (BIODESIGN International, Saco, ME, and Bio-Rad Laboratories, Hercules, CA); rabbit and mouse IgG TrueBlot (eBioscience, San Diego, CA); highly cross-absorbed Alexa 488 goat anti-mouse and anti-human IgG and Alexa 594 goat anti-rabbit IgG (Molecular Probes, Eugene, OR).

### *Immunoprecipitation and Mass Spectrometry*

L2 cells were lysed with ice-cold lysis buffer (0.5% Triton X-100 [TX-100], 10 mM Tris-HCl, pH 7.6, 150 mM NaCl, 1 mM EDTA supplemented with 1× Complete, EDTA-free proteinase inhibitor cocktail [Roche, Indianapolis, IN]), 50 mM NaF and 1 mM sodium vanadate), and immunoprecipitation was carried out with anti-ARH, anti-dynein IC, mouse or preimmune IgG (5 $\mu$g) as previously described (Lehtonen *et al.*, 2004). As a control, the ARH IgG was immunodepleted by preincubation with GST-ARH fusion protein before immunoprecipitation. Bound proteins were separated by 8% SDS-PAGE and stained with GelCode Blue (Pierce, Rockford, IL), and the bands in the ARH immunoprecipitates were processed for mass spectrometry as described earlier (Zhou *et al.*, 2004).

### *Pulldown Assays and Immunoblotting*

GST-ARH fusion proteins were expressed in *Escherichia coli* BL21(DE3) (Stratagene; La Jolla, CA), purified on glutathione-Sepharose beads (Amersham Bioscience, Piscataway, NJ), and used for pulldown assays on cell lysates. Immunoblotting using HRP-conjugated antibodies and ECL was done as described previously (Lehtonen *et al.*, 2004). Alternatively, proteins were transferred to polyvinylidene difluoride-FL membranes (Millipore, Bedford, MA), blocked with Odyssey blocking buffer (Li-COR Biotechnology, Lincoln, NE) diluted 1:1 with phosphate-buffered saline (PBS), and incubated with primary antibodies and Alexa 680 (Molecular Probes) or IR 800 goat anti-rabbit or anti-mouse IgG (Rockland Immunochemicals, Gilbertsville, PA) followed by detection and quantification with an Odyssey Infrared Imager (Li-COR Biotechnology).

### *Cell Fractionation*

L2 cells were homogenized by passage (10 times) through a 30-gauge needle in ice-cold homogenization buffer (10 mM Tris-HCl, pH 7.6, 150 mM NaCl, 1 mM EDTA, 1× Complete, 50 mM NaF, 1 mM sodium vanadate). Nuclei were removed by centrifugation (1000 × *g* for 5 min). Membrane and cytosolic fractions were prepared by centrifugation of a postnuclear supernatant (PNS) in a Beckman TLA45 rotor (Fullerton, CA) at 100,000 × *g* at 4°C for 1 h. For coimmunoprecipitation experiments the cytosolic fraction was adjusted to 0.5% TX-100, and the membrane pellet was resuspended in an equal volume of lysis buffer.

For cosedimentation experiments, L2 cells were homogenized as above in 0.3 M sucrose, 25 mM imidazole, pH 7.2, 1 mM EDTA (Marples *et al.*, 1998) with 1× Complete, 50 mM NaF, and 1 mM sodium vanadate. Seven hundred micrograms PNS or cytosolic fraction prepared as above were applied to the top of a 15–40% continuous sucrose gradient. Sucrose solutions were prepared in 25 mM imidazole, pH 7.2, 1 mM EDTA with 1× Complete. After centrifugation in an SW 40 rotor at 40,000 rpm at 4°C for 16 h, fractions were collected from the top and prepared for immunoblotting.

### *Immunoisolation*

Sucrose fractions 8–10 (obtained as described above) containing ARH, dynein HC and IC, and $\gamma$-tubulin were combined and incubated with ARH IgG or protein A–purified preimmune serum or immunodepleted ARH IgG prebound to protein A-Sepharose beads. Beads were then washed (5×, 5 min each) in 0.3 M sucrose, 25 mM imidazole, pH 7.2, 1 mM EDTA supplemented with 1× Complete, 50 mM sodium fluoride, and 1 mM sodium vanadate. The nonbound fraction and wash solutions from each sample were collected and pelleted by centrifugation (100,000 × *g* at 4°C for 1 h). Samples were boiled in Laemmli sample buffer and prepared for immunoblotting.

### *Indirect Immunofluorescence*

Cells were fixed with −20°C acetone or methanol for 10 min or −20°C methanol followed by −20°C acetone, blocked with 1% bovine serum albumin (BSA), and incubated with primary antibodies diluted in 0.1% BSA in PBS for 1 h at room temperature. Detection was with Alexa 488 goat anti-mouse or Alexa 594 goat anti-rabbit IgG in 0.1% BSA in PBS (1 h). For IF of ARH truncation mutants, HeLa cells were prepermeabilized with 0.5% TX-100 (10 s) before fixation. To disrupt microtubules, cells were treated with 1 $\mu$g/ml nocodazole for 90 min at 37°C and prepermeabilized with 0.1% TX-100 vol/vol, 80 mM Pipes, pH 6.8, 5 mM EGTA, and 1 mM $MgCl_2$ for 1 min at room temperature. For microtubule reformation assays, wt or $Arh^{-/-}$ MEFs were treated with nocodazole (5 $\mu$g/ml, 90 min), rinsed (5×) with PBS, and incubated at 37°C for 5, 10, or 20 min to allow reformation of microtubules. Samples were mounted in 75% glycerol in PBS containing 1 mg/ml paraphenylinediamine and examined with a Zeiss AxioImager M1 microscope using a Zeiss 63× oil immersion objective (na = 1.35; Carl Zeiss, Thornwood, NY). Images were collected with an ORCA-ER camera (Hamamatsu, Bridgewater, NJ) using Scion image version 1.59 Openlab (Improvision, Lexington, MA) and processed using Adobe Photoshop 5.5 or Adobe Photoshop 7.0 (Adobe Inc., San Jose, CA).

### *Isolation of Centrosomes*

Centrosomes were isolated from rat-1 cells according to previously described protocols (Mitchison and Kirschner 1986; Bornens *et al.*, 1987). Briefly, confluent cultures pretreated with nocodazole (5 $\mu$g/ml) and cytochalasin D (2 $\mu$M) for 1 h at 37°C (to release centrosomes that otherwise sediment with the nuclear pellet; Mitchison and Kirschner, 1986; Blomberg-Wirschell and Doxsey, 1998) were lysed in 1 mM HEPES, pH 7.2, 0.5% NP-40, 0.5 mM $MgCl_2$, 0.1% $\beta$-mercaptoethanol, 1 mM PMSF, and 1× Complete. Nuclei were removed by centrifugation, and the resulting PNS containing the centrosomes was loaded onto a 60% sucrose (wt/wt) cushion and centrifuged (1 h at 8000 rpm) in a Beckman JA-20 rotor. Aliquots from the loading region (C1), the cushion interface (C2), and within the cushion (C3) were saved. The remaining C2 (3 ml) was loaded on top of a discontinuous sucrose gradient (40, 50, and 70%, wt/wt) containing 0.5% TX-100 and centrifuged (25,000 rpm for 1 h in a SW40 rotor). Thirteen fractions (1 ml each) were collected from the top, diluted with 10 mM Pipes buffer, and sedimented (25,000 rpm for 1 h in a SW40 rotor), and the bottom 100 $\mu$l was collected. The 50–70% sucrose interface (corresponding to fraction 9 in our experiments) represents the centrosome-enriched fraction (Mitchison and Kirschner, 1986; Bornens *et al.*, 1987) and also contained the biggest peak of sedimentable $\gamma$-tubulin.

### *Preparation and Expression of ARH Truncation Mutants*

Rat ARH full-length cDNA (aa 1–307) and truncated forms (aa 1–177, 28–174, 43–174 and 175–307) were obtained by PCR using rat ARH (XM_575931) cloned in pcDNA 3.1 as a template. The PCR products were subcloned into the EcoRI and XhoI sites of pCMV-Myc (BD Biosciences, San Jose, CA) resulting in N-terminal myc-tagged constructs. DNA sequences were verified by sequencing. The constructs were transiently transfected into HeLa cells using GeneJuice (Novagen/EMD Biosciences, Madison WI) or Fugene 6 (Roche) and analyzed by indirect immunofluorescence (IF) or immunoprecipitation (IP) 48 h after transfection. For immunoprecipitation, cells were lysed in IP buffer containing 0.5% TX-100, and co-IP was performed using 1 $\mu$g anti-myc antibody as described above.

### *Centrosome Area, Intensity, and Volume Measurements*

Indirect IF using anti γ-tubulin IgG and DAPI was carried out on wt and *Arh*$^{-/-}$ MEFs as outlined above using exactly the same conditions for staining and image acquisition. For area measurements, ~50 fields were recorded in a random manner for each cell type using the same settings. To eliminate bias the DAPI channel was used to choose suitable fields. The images were thresholded to remove background, and the number of centrosomes and their area and fluorescence intensity were measured using Adobe Photoshop. For centrosome volumetric measurements images were acquired with an Olympus FluoView FV1000 confocal microscope using a 60× objective lens (Olympus, Melville, NY). *Z*-slices at 0.5 μm with 0.05-μm *z*-steps were acquired. For each cell type ~20 γ-tubulin–stained cells were recorded and 3D rendering and volume measurements for centrosomes in each field were performed using Image ProPlus and 3D Constructor (Media Cybernetics, Bethesda, MD).

### *Depletion of ARH by Small Interfering RNA*

Rat-1 cells, ~8 × 10$^4$, were seeded in 12-well plates 20–24 h before transfection. Cells were transiently transfected with 100 nM rat smartpool ARH small interfering RNA (siRNA; Dharmacon, Lafayette, CO, M-101542–00, LOC500564) or scrambled siRNA (Dharmacon, D-001210-01 or D-001206-13), using 2 μl Lipofectamine 2000 (Invitrogen, Carlsbad, CA) per well. Forty-eight hours after transfection the cells were lysed and immunoblotted for ARH, actin, total histone-H3, and phosphohistone-H3 or prepared for IF. For rescue experiments, rat-1 cells transfected with siRNA were infected 15 h later with pMSCV (mouse stem cell virus) full-length human ARH or mock virus as previously described (Nagai *et al.*, 2003) and analyzed 48 h later by immunoblotting.

### *Growth Measurements*

Cells (n = 20,000; wt or *Arh*$^{-/-}$ MEFs) were plated per well (six-well plates), and the cells were counted at 24, 48, 72, and 96 h. For each time point, three wells each of the wt and *Arh*$^{-/-}$ cells were trypsinized, and the number of cells in each suspension was counted using a Neubauer hemocytometer (Fischer Scientific, Pittsburgh, PA). Each count was performed in duplicate, and the mean was used for statistical purposes. The mean ± SE of the triplicate samples for each time point were plotted against time. For growth measurements after siRNA transfection, rat-1 cells transfected with rat ARH or scramble siRNA were trypsinized and counted 48 h after transfection. For rescue experiments, the siRNA-treated cells were transiently transfected 15 h after siRNA transfection with human ARH-EGFP-N1 or EGFP-N1 using Fugene 6, and the cells were counted 48 h later. The expression of human ARH-GFP and GFP alone in rat-1 cells was confirmed by immunoblotting.

### *Time-Lapse Imaging and Statistical Analysis of Cytokinesis*

Wild-type and *Arh*$^{-/-}$ MEFs were analyzed for cytokinesis defects by differential interference contrast time-lapse microscopy using a DeltaVision RT microscope (Applied Precision, Issaquah, WA) equipped with a heated stage and a humidified 5% $CO_2$ infusion system (UCSD Neuroscience Shared Microscopy Facility). Images from 30 to 40 fields were recorded every 2 or 3 min for up to 15 h using an automated motorized stage and a 25× differential interference objective. Mitotic events were observed, and the duration of cytokinesis was recorded. The beginning of anaphase (which is a more well-defined and consistently visible event in these cells) was used as the starting point for recording the duration of cytokinesis. In several instances in the *Arh*$^{-/-}$ MEFs, cytokinesis lasted >5 h (>10 h in some cases) and was incomplete even when the automated recording ended; for a conservative estimate of the duration of cytokinesis in such cases, the end point of the recording was used as the end point of cytokinesis. The mean duration of cytokinesis of ARH-depleted cells versus controls was compared using Student's *t* test. In reversal experiments, *Arh*$^{-/-}$ MEFs were infected with mock pMSCV-virus or pMSCV virus expressing full-length human ARH (Nagai *et al.*, 2003). Twenty-four hours later, time-lapse movies were recorded and statistical analysis for duration of cytokinesis was carried out as described above.

## RESULTS

### *ARH Forms a Multiprotein Complex with Dyneins and γ-Tubulin Complex Proteins*

To identify new ARH-interacting partners, we carried out immunoprecipitation on L2 cell lysates with protein A–purified ARH (3393) IgG. The anti-ARH IgG specifically coimmunoprecipitated seven protein bands not observed in immunoprecipitates obtained with preimmune serum or immunodepleted ARH IgG (Figure 1A). By mass spectrometry the >250-kDa bands were identified as dynein HC, the ~75- and ~65-kDa bands as dynein IC, and the <100-kDa bands as GCP2 and GCP3. The 34-kDa band was ARH itself.

Dyneins are motor proteins involved in trafficking of endocytic vesicles and retrograde cargo along microtubules as

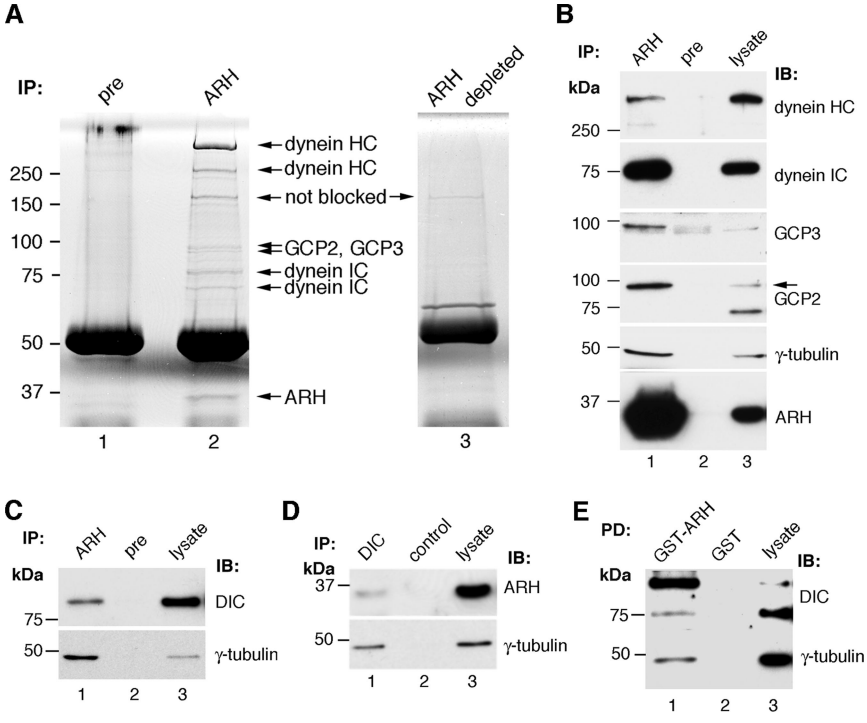


**Figure 1.** Identification of ARH interaction partners by mass spectrometry. (A) GelCode Blue–stained gel of immunoprecipitates obtained with ARH (lane 2), preimmune (lane 1), or immunodepleted ARH IgG (lane 3). Bands present only in the ARH precipitates (arrows) were identified by mass spectrometry as dynein HC, dynein IC, GCP2, and GCP3. The 34-kDa band is ARH itself. L2 cell lysate (2.6 mg) was incubated with protein A–purified ARH 3393, preimmune, or anti-ARH 3393 IgG immunodepleted with GST-ARH fusion protein (ARH depleted, lane 3). Immune complexes were bound to protein A-Sepharose, separated by 8% SDS-PAGE, and stained with GelCode Blue. Three immunoprecipitates were combined per lane. (B) Immunoblots showing dynein HC, dynein IC, GCP3, GCP2, and γ-tubulin in immunoprecipitates obtained with ARH (lane 1) but not preimmune (pre, lane 2) IgG. Lane 3, L2 cell lysate (25 μg, dyneins, GCP2, and ARH; 100 μg, γ-tubulin; 200 μg GCP3). The arrow indicates the expected size of GCP2. (C) Dynein IC and γ-tubulin are also specifically immunoprecipitated with a second ARH (3392) IgG (lane 1) but not with preimmune IgG (lane 2). Lane 3, L2 cell lysate (5 μg). (D) ARH and γ-tubulin are immunoprecipitated with dynein IC (DIC) IgG (lane 1), but not with control mouse IgG (lane 2). Lane 3, L2 cell lysate (5 μg). (E) Dynein IC and γ-tubulin are pulled down with GST-ARH (lane 1), but not with GST alone (lane 2). Lane 3, L2 cell lysate (5 μg dynein IC; 25 μg γ-tubulin).

well as in spindle dynamics and other steps in mitosis through their microtubule-associated functions (Karki and Holzbaur, 1999; Vallee *et al.*, 2004). GCP2 and GCP3 together with γ-tubulin are part of the γ-TUSC, which is believed to be a subunit of the larger γ-TuRC, which functions to nucleate microtubules at the centrosome (Doxsey *et al.*, 2005). A common characteristic of dynein subunits and γ-TuRC protein components is that they localize to the centrosome and have been implicated in the assembly of centrosome components (Young *et al.*, 2000).

The presence of dynein HC, dynein IC, GCP2, and GCP3 in ARH complexes in L2 cells was confirmed by immunoblotting (Figure 1B). Similar results were also obtained on rat-1 cell lysates (data not shown). We also tested for γ-tubulin (GCP1), a major component of γ-TuRC, and confirmed its presence in ARH immunoprecipitates (Figure 1B). The γ-tubulin band was not detected in the original GelCode Blue–stained gels processed for mass spectrometry (Figure 1A), presumably because it runs at approximately the same location as IgG heavy chain (48 kDa). We were unable to detect components of the dynactin complex (p50 or the $p150^{glued}$ subunits), which function closely with dynein (Schroer, 2004) in ARH immunoprecipitates.

The association of ARH with dyneins and γ-tubulin complex proteins was confirmed by immunoprecipitation on L2 cell lysates with 1) a second ARH antibody, ARH 3392 IgG (Figure 1C) and 2) a dynein IC antibody (Figure 1D). Furthermore, both dynein IC and γ-tubulin were pulled down with GST-ARH (but not GST alone) from L2 cell lysates (Figure 1E). Taken together these results verify the mass spectrometry findings regarding the interactions of ARH with these proteins.

### *ARH, Dyneins, and γ-Tubulin Associate in Membrane Fractions and on Immunoisolated Vesicles*

We next analyzed if ARH and its interaction partners form a complex on membranes and/or in the cytoplasm. ARH, dyneins, γ-tubulin, GCP2, and GCP3 were all present in both membrane (100,000 × *g* pellet; P100) and cytosolic (100,000 × *g* supernatant; S100) fractions prepared from L2 cells (Figure 2A) and were found in immunoprecipitates obtained from both membrane and cytosolic fractions (Figure 2B).

To further analyze the protein complexes we carried out cosedimentation analysis by sucrose gradient centrifugation of PNS from L2 cells. ARH, dyneins, and γ-tubulin complex proteins cosedimented in sucrose gradients (Figure 3A). They peaked in fractions 2 (soluble fraction) and 9–10 (membrane fractions; Figure 3A). The recycling endosome markers syntaxin 13 and Rab11 which colocalize with ARH in L2 cells (Nagai *et al.*, 2003) were found in membrane fractions 8–13, clathrin in fractions 2–3, and the early endosome marker EEA1 in fractions 1–2 and 8–10 (Figure 3A). Thus ARH cosediments in membrane fractions enriched in γ-tubulin, GCP2 and GPC3, and EEA1, but not with clathrin, which is detected exclusively in the soluble fractions under these conditions. These fractions would not be expected to contain centrosomes because under these conditions centrosomes sediment with the nuclei (Mitchison and Kirschner, 1986; Blomberg-Wirschell and Doxsey, 1998).

To determine whether ARH, dyneins and γ-tubulin are found on the same vesicles, we combined membrane fractions 8–10, where ARH, dyneins, and γ-tubulin cosediment, and carried out immunoisolation with ARH antibodies bound to protein A-Sepharose beads. A pool of dynein IC and γ-tubulin was found on the bound fractions (Figure 3B, lane 1), whereas the recycling endosome markers syntaxin 13 and Rab11 was detected only in the nonbound fractions. No dynein IC or γ-tubulin was detected with preimmune IgG or immunodepleted ARH IgG (Figure 3B, lane 3).

To summarize, ARH, dynein, and γ-tubulin complex proteins form a complex both in the cytosol and on membranes, they cosediment in membrane fractions in sucrose gradients and are found on the same vesicles after immunoisolation.

### *ARH Colocalizes with Several Centrosome Markers at Centrosomes*

Because we found that ARH forms a complex with a set of proteins that are known to localize to the centrosome and the mitotic apparatus, we next investigated whether ARH is localized on centrosomes. Immunofluorescence (IF) on L2 (Figure 4, A–C) and rat-1 (Figure 4, D–F) cells fixed with methanol/acetone (optimal for centrosome analysis) revealed that ARH colocalizes with the centrosome marker γ-tubulin (Figure 4, A–C), with dynein IC (Figure 4, D–F), also a centrosomal protein, and with pericentrin (data not shown), another centrosome marker. The centrosomal localization of ARH was also confirmed using an ARH IgG from Dr. Linton Traub (Figure S1). In addition to L2 and rat-1 cells, ARH was found to localize to the centrosome in BAEC,

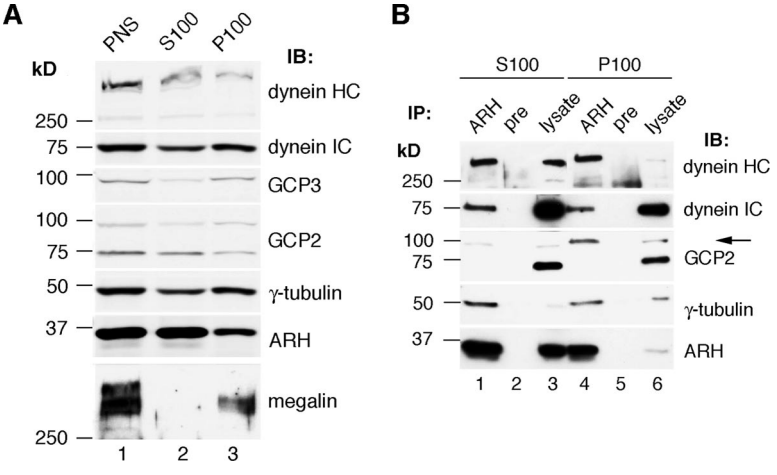


**Figure 2.** ARH, dyneins, and γ-tubulin complex proteins interact in both membrane and cytosolic fractions. (A) ARH and its interaction partners, dynein HC, dynein IC, GCP2, GPC3, and γ-tubulin, are found in both membrane (P100, lane 3) and cytosolic (S100, lane 2) fractions from L2 cells. Megalin, an integral membrane protein that binds ARH, is detected exclusively in the membrane fraction (lane 3) as expected. L2 cells were homogenized in immunoprecipitation buffer lacking detergent, and the PNS (lane 1) was fractionated into cytosolic (S100, lane 2) and membrane (P100, lane 3) fractions. Equal volumes of the fractions were analyzed by immunoblotting with the indicated antibodies. (B) Dynein HC, dynein IC, GCP2, and γ-tubulin can be co-IPed with ARH IgG from both cytosolic (S100, lane 1) and membrane (P100, lane 4) fractions. None of these proteins were detected after precipitation with preimmune IgG (lanes 2 and 5). Lanes 3 and 6, lysates of cytosolic and membrane fractions (25 μg). Immunoprecipitation was carried out with ARH 3393 or preimmune IgGs on cytosolic (100,000 × *g* supernatant) and membrane (100,000 × *g* pellet) fractions and immunoblotted with the indicated antibodies.

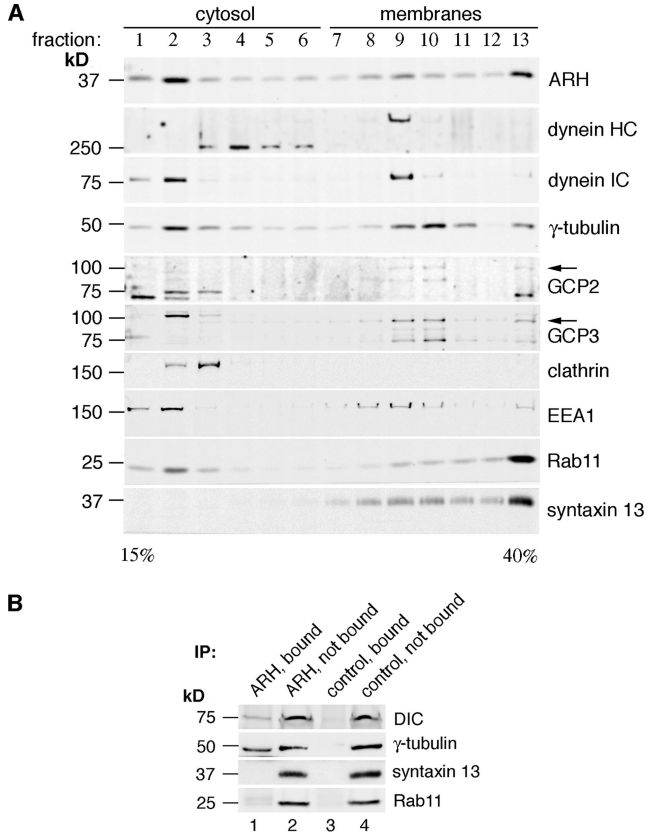


**Figure 3.** ARH, dyneins, and γ-tubulin complex proteins cosediment and are found on immunoisolated membranes. (A) ARH, γ-tubulin, dynein, GCP2, and GCP3 peak in both soluble (fractions 2–4) and membrane (fractions 9–10) fractions in continuous sucrose gradients. The early endosome marker EEA1 also peaks in the same fractions. Clathrin is found exclusively in the soluble fractions (fractions 2 and 3). Arrows indicate the expected size of GCP2 and GPC3. The PNS from L2 cells was loaded on top of a 15–40% continuous sucrose gradient and centrifuged as described in *Materials and Methods*. One-milliliter fractions were collected from the top, and equal volumes of each were immunoblotted as indicated. (B) Dynein IC (DIC) and γ-tubulin are found both on vesicles immunoisolated with ARH IgG (ARH, bound; lane 1), and in nonbound fractions (ARH, nonbound; lane 2). Recycling endosome markers syntaxin 13 and Rab11 are not detected in the bound fraction. Membrane fractions 8–10 obtained by sucrose gradient fractionation as in A were combined and incubated with ARH 3393 IgG or preimmune IgG (control) prebound to protein A-Sepharose beads for 4 h. Bound and nonbound subfractions were analyzed by immunoblotting.

HeLa cells (Figure S1) and retinal pigment epithelial cells, indicating that the centrosomal association of ARH is not limited to just one or two cell types.

To test whether the centrosomal pattern of immunostaining of ARH is dependent on an intact microtubule network, we treated rat-1 cells with the microtubule-disrupting drug nocodazole and immunostained for ARH and γ-tubulin. The centrosomal localization of ARH and γ-tubulin seen in untreated rat-1 cells (Figure 4, G–J) persisted after disruption of microtubules with nocodazole (Figure 4, K–N). Taken together, the colocalization of ARH with centrosome markers in multiple cell types and its persistence on centrosomes after nocodazole treatment indicate that ARH is a bona fide centrosomal protein.

### *ARH Cofractionates with γ-Tubulin on Isolated Centrosomes*

To further investigate the association of ARH with centrosomes, we isolated centrosomes by fractionation of rat-1 cells using standard protocols (Mitchison and Kirschner, 1986; Bornens *et al.*, 1987). The majority of the cellular ARH was in the nonsedimentable form (C1; Figure 5A); however, ~1% of the total was recovered from a 60% wt/wt sucrose cushion interphase (C2), which contains intact centrosomes. This fraction was further centrifuged in a discontinuous sucrose gradient to prepare an enriched centrosomal fraction located at the 50–70% sucrose interface (fraction 9 of the gradient; Mitchison and Kirschner, 1986; Bornens *et al.*, 1987). The largest peaks of ARH and γ-tubulin were found in fraction 9 (Figure 5B), confirming the cosedimentation of ARH with γ-tubulin and further verifying the presence of ARH on centrosomes. As a negative control, no Rab11 was detected in the centrosome fraction (data not shown). A sample of the isolated centrosomal fraction was spotted on a slide and stained for ARH and γ-tubulin. By IF many of the structures stained positively for ARH as well as for γ-tubulin (Figure 5, C and D) but not for Rab5, used as a negative control (Figure 5E).

### *The N-Terminus of ARH Is Necessary for Its Centrosomal Targeting/Retention*

ARH possesses a number of conserved modular domains, including "a Dab-1-like" PTB domain (Stolt and Bock, 2006) and clathrin, AP2, and PDZ (PIM) binding domains (Wilund *et al.*, 2002; Cohen *et al.*, 2003). To pinpoint the region required for centrosomal targeting, we evaluated the localization of full-length ARH and myc-tagged truncation mutants covering aa 1–177 and 175–307 (Figure 6A). Full-length ARH (Figure 6B) and $ARH_{1–177}$ (Figure 6C) localized to centrosomes, whereas $ARH_{175–307}$ did not (Figure 6D). Truncation mutants smaller than 1–177 ($ARH_{28–174}$ and $ARH_{43–174}$) failed to localize to centrosomes (see Figure 8, A and B). These findings indicate that aa 1–177, dominated by the PTB domain (43–177), is necessary and sufficient for targeting of ARH to the centrosome, whereas the C-terminus (including the clathrin, AP-2, and PIM-binding domains) is dispensable in mediating its targeting.

### *ARH Localizes to Components of the Mitotic Machinery in a Cell-Cycle–dependent Manner*

A number of centrosome proteins exhibit cell cycle–dependent, dynamic behavior in that they are sequentially present at more than one location on the mitotic apparatus. We found that ARH undergoes a similar dynamic behavior in mitotic cells (Figure 7). In mitotic rat-1 cells ARH was first detected surrounding the nuclear envelope in early prophase, where it colocalized with the dynactin complex protein $p150^{glued}$ (Figure 7A). It then sequentially accumulated in a spotlike manner on kinetochores (Figure 7, B and C) as confirmed by colocalization with dynein IC (Figure 7B), known to concentrate on kinetochores, and by a human anti-centromere Ig (Figure 7C). On progression of mitosis, ARH was observed at both kinetochores and spindle poles, which were specifically stained with γ-tubulin (Figure 7D). At metaphase ARH was also found at the spindle poles labeled with γ-tubulin (Figure 7E), but by the end of anaphase/beginning of telophase there was little, if any, ARH detectable at the spindle poles (Figure 7F, arrowheads). Rather, ARH was found on punctate structures in the cytoplasm. Interestingly, during cytokinesis ARH localized to the midzone where it colocalized with dynein IC. Midzone

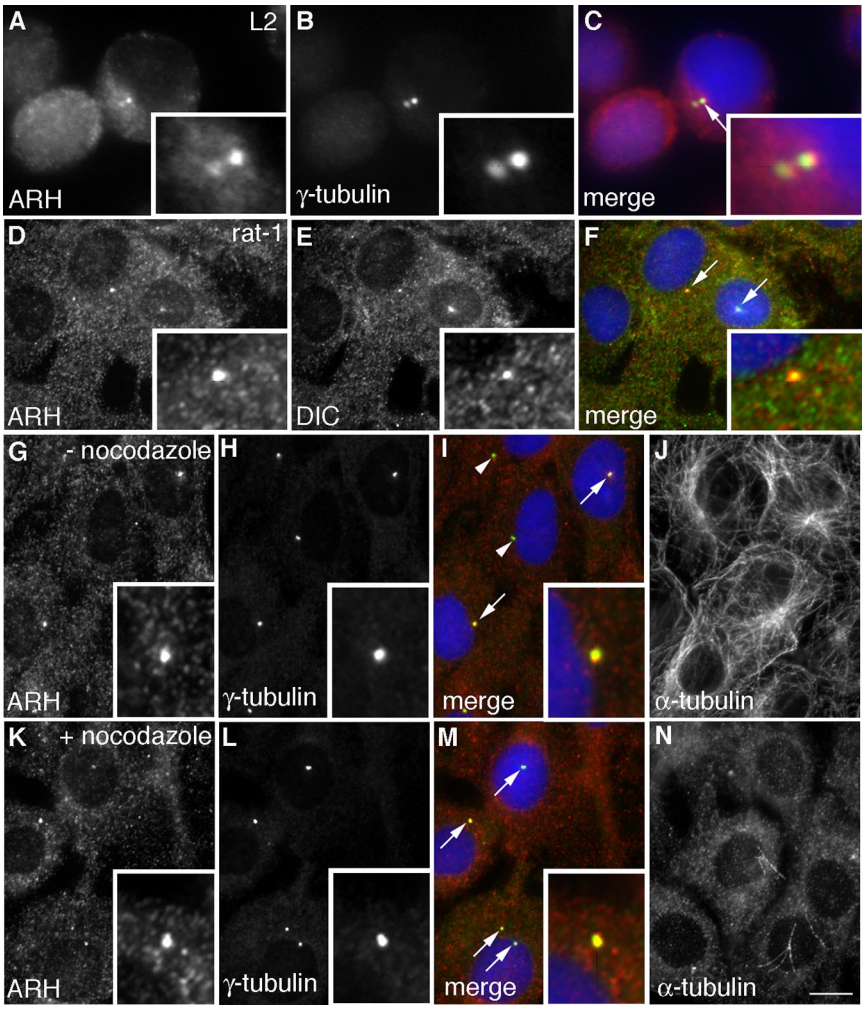


**Figure 4.** ARH colocalizes with γ-tubulin and dynein IC on centrosomes. (A–C) ARH and γ-tubulin colocalize (yellow) on centrosomes in L2 cells (arrow in the merged image) that are enlarged in the inset. L2 cells were fixed with acetone and stained for ARH, γ-tubulin, and DAPI. (D–F) ARH and dynein IC (DIC) similarly colocalize on centrosomes (arrows) in rat-1 fibroblasts. (G–N) Field of cells showing colocalization of ARH with γ-tubulin (arrows) in both control (− nocodazole) (I) and nocodazole treated (+ nocodazole) (M) cells. (J and N) α-Tubulin staining verifies that the filamentous network of microtubules was disrupted by nocodazole treatment. Centrosomes are enlarged in the insets. Untreated cells or those treated with nocodazole (1 μg/ml, 90 min; K–N) were fixed with methanol followed by acetone and stained as indicated. Bar: (A–C) 3 μm; (D–N) 6.5 μm.

staining was best visualized in HeLa (Figure 7, G and H) and RPE cells (not shown). These data suggest dynamic trafficking of ARH along the mitotic apparatus, which might reflect a role for ARH during mitosis.

### *Overexpression of Truncated Forms of ARH or Depletion of ARH Results in Defects in Centrosome Assembly*

During our analysis of the targeting of ARH truncation mutants we noted that in cells expressing $ARH_{28–174}$ and $ARH_{43–174}$ lacking the extreme N-terminus of ARH, centrosomes were either absent or were distinctly smaller than those in untransfected cells (Figure 8, A and B). To determine if this was due to failure to form complexes with centrosomal proteins, we tested the ability of the truncation mutants to interact with γ-tubulin in co-IP experiments. When these constructs were expressed in HeLa cells (Figure 8I), both truncated forms were able to interact with γ-tubulin to the same extent as full-length ARH or $ARH_{1–177}$, whereas $ARH_{175–307}$, lacking the PTB domain did not interact. Our findings that $ARH_{28–174}$ and $ARH_{43–17}$ interacted with γ-tubulin but did not localize to centrosomes suggested that these mutants might have a dominant negative effect by competing with endogenous ARH and sequestering γ-tubulin (and possibly other centrosome components) in the cytoplasm, thus preventing them from assembling at the centrosome.

We reasoned that if ARH is involved in centrosome assembly defects in centrosomes might be seen when ARH is absent. To explore this possibility, we analyzed centrosomes in wt and $Arh^{-/-}$ MEFs using three different centrosome markers (γ-tubulin, pericentrin, and centrin2). We found that in $Arh^{-/-}$ MEFs centrosomes were smaller or there was a total absence of centrosomes (Figure 8, F–H). To quantify this effect we carried out a 3D reconstruction of centrosomes in wt and $Arh^{-/-}$ MEFs stained with γ-tubulin (Figure 8, C–H) and measured the volume of centrosomes by confocal microscopy (Table 1). We found significant differences: ~25% of the $Arh^{-/-}$ cells had no detectable centrosomal staining, the mean centrosome number was reduced 20–40%, and the mean centrosome volume per cell was reduced by up to 64%. These results document that $Arh^{-/-}$ MEFs contain fewer centrosomes and that those that are present are smaller in size and stain less intensely for γ-tubulin, indicating that ARH may be required for centrosome assembly.

We also investigated the possibility that ARH plays a role in the anchoring and/or nucleation of microtubules from the centrosome but found that the rate of microtubule reformation after washout of nocodazole was comparable in wt and $Arh^{-/-}$ MEFs (Figure S2). We conclude that although ARH appears to be necessary for centrosome maturation, it does not seem to be required for microtubule nucleation at centrosomes in these cells.

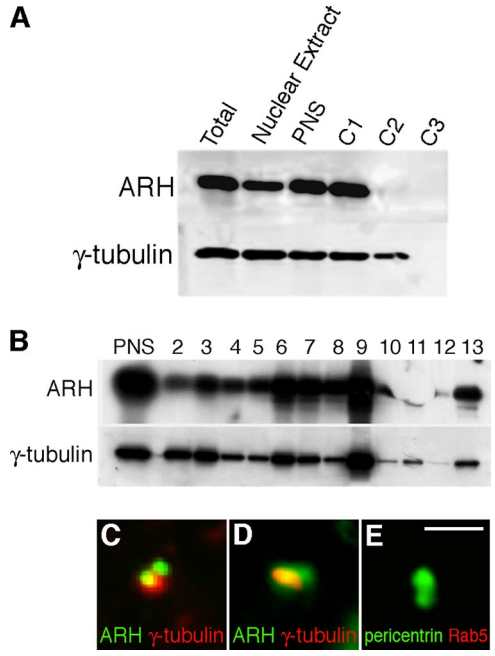


**Figure 5.** ARH is found on isolated centrosomes. (A) Centrosomes were isolated from rat-1 cells by cenrifugation of a PNS onto a 60% sucrose cushion as described in *Materials and Methods.* Aliquots (0.1%) of each of the cell lysate (Total), PNS, loading region (C1), 60% cushion interface (C2), and 60% sucrose cushion (C3) were immunoblotted for ARH and γ-tubulin. Most of the ARH is soluble (C1) and does not enter the C2 cushion, which contains the centrosomes. (B) C2 was loaded on top of a 40–50 to 70% (wt/wt) discontinuous sucrose gradient and centrifuged as described in *Materials and Methods.* The gradient fractions were collected and immunoblotted for ARH and γ-tubulin. The highest concentration of the sedimentable ARH and γ-tubulin is found in fraction 9 (50–70% sucrose interface), which represents the centrosome-enriched fraction. (C–E) The centrosome-enriched fraction was spotted on a coverslip, fixed with methanol, and labeled for ARH (red) and γ-tubulin (green), which colocalize in centrosomes (yellow) in these merged images (C–D). (E) As a control, the centrosome-enriched fraction was labeled with Rab5 (red) which did not colocalize with pericentrin (green). Bar, 1.5 μm.

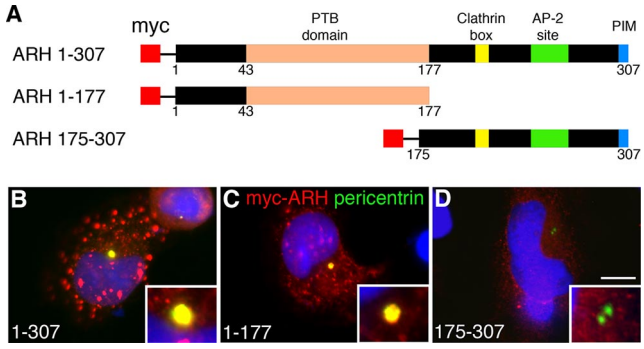


**Figure 6.** The N-terminus of ARH including the PTB domain is required for targeting to centrosomes. (A) Bar diagrams showing myc-tagged full-length $ARH_{1–307}$ and truncated forms of ARH used for mapping. Full-length $ARH_{1–307}$ (B) and $ARH_{1–177}$ (red; C) are targeted to centrosomes and colocalize (yellow) with pericentrin (green) on centrosomes whereas $ARH_{175–307}$ (D) does not. Insets, higher magnification of centrosomes. ARH constructs were transiently expressed in HeLa cells, prepermeabilized with TX-100, fixed with methanol, and stained for myc to detect ARH, pericentrin (centrosomal marker), and DAPI (blue). Bar, 12 μm.

### *ARH Affects the Rate of Cell Growth*

Next we investigated whether ARH plays a role in cell cycle progression through interphase and mitosis by checking phosphohistone-H3 levels and cell growth in rat-1 cells transfected with rat Smartpool ARH siRNA. We found that phosphohistone-H3 but not total histone-H3 was reduced 55–85% in ARH-depleted cells compared with controls (Figure 9, A and B), indicative of reduced entry of ARH-depleted cells into mitosis. We confirmed that this effect was due to reduced levels of ARH by showing that full-length human ARH introduced by retroviral infection into rat ARH siRNA-treated cells partially restored phosphohistone-H3 levels (Figure 9, C and D). In ARH siRNA-treated cells expressing mock virus, phosphohistone-H3 was reduced 33–45%, whereas in cells expressing human ARH phosphohistone-H3 was reduced 5–33% (Figure 9, C and D).

To determine if down-regulation of ARH affects the rate of cell growth, we counted the cells after ARH depletion and found that the number of cells/well in ARH siRNA-treated cells was 53–64% of the scramble control (Figure 9E), consistent with a role for ARH in regulating the cell cycle. This effect was partially reversed by introducing human ARH-GFP into the cells treated with rat ARH siRNA: The number of cells/well in ARH siRNA-treated cells expressing human ARH-GFP was 73–78% of the scramble control, whereas the number of cells/well was 58–64% of the scramble control in rat ARH siRNA-treated cells expressing GFP alone (Figure 9E). The rescue was only partial in keeping with the fact that the transfection efficiency of hARH-GFP was ~20–25%. In addition, we checked the growth rate of MEFs and found that $Arh^{-/-}$ MEF cells grew at a significantly slower rate than wt MEFs (Figure 9F).

### *ARH Deficiency Results in Prolonged or Incomplete Cytokinesis*

To further evaluate the defect of ARH depletion on mitosis and cytokinesis, we performed time-lapse, differential interference contrast imaging on wt and $Arh^{-/-}$ MEFs and noted a striking delay in cytokinesis. The vast majority (~70%) of the wt MEFs completed cytokinesis in <2 h, whereas <20% of the $Arh^{-/-}$ cells completed cytokinesis during this same time period (Figure 10D). Nearly one-third of the cytokinesis events in $Arh^{-/-}$ cells took 5 h or longer, and many failed to complete cytokinesis and stayed connected by long persistent cytoplasmic bridges. The mean duration of cytokinesis in wt MEFs was 104.2 ± 4.4 min (mean ± SE, n = 57) compared with at least 248.6 ± 19.9 min (mean ± SE, n = 44) in $Arh^{-/-}$ cells. (Because many $Arh^{-/-}$ cells had not completed division by the end of the data collection period, the mean for the $Arh^{-/-}$ cytokinesis is actually a conservative estimate.) When human Arh was introduced into $Arh^{-/-}$ MEFs, the mean time for cytokinesis was reversed, back to 117 ± 8.8 min compared with controls (mock infected cells) that had a mean cytokinesis time of 209 ± 16.9 min (Figure 10E). Figures 10, A–C, show typical examples of time-lapse images of mitosis in wt (Figure 10A) and $Arh^{-/-}$ (Figure 10B) cells and a reversal of the cytokinesis defect in the $Arh^{-/-}$ MEFs upon infection with pMSCV-ARH retrovirus (Figure 10C). (Movies corresponding to these frames and additional examples of cytokinesis defects are available in Supplemental Materials as Video 1, wt; Video 2, $Arh^{-/-}$; Video 3, wt; Video 4, $Arh^{-/-}$; Video 6, $Arh^{-/-}$ with mock infection; and Video 7, $Arh^{-/-}$ with pMSCV-ARH infection). MEF cells also showed early cytokinesis defects characterized by the abrupt termination of mitosis and the rapid

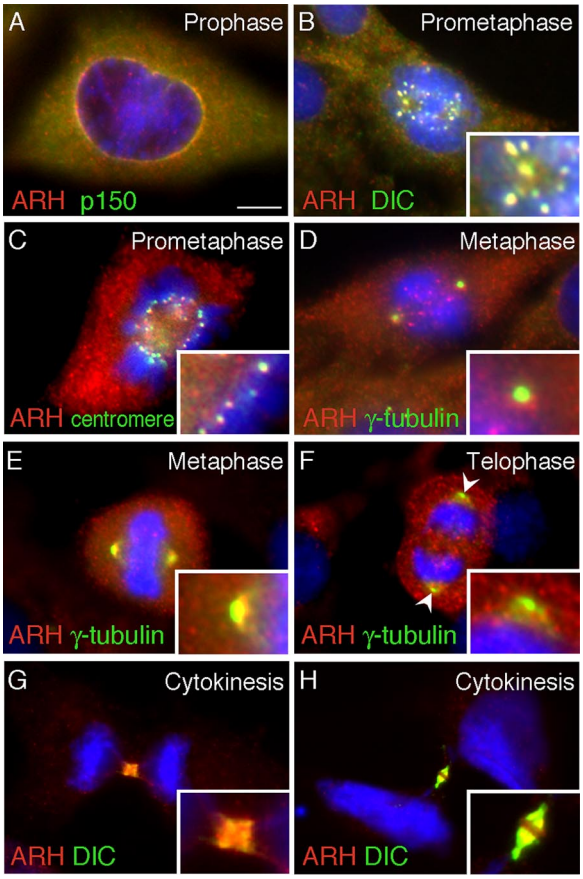


**Figure 7.** ARH localizes sequentially to the nuclear envelope, kinetochores, spindle poles, and midbody during mitosis. At the onset of prophase (A) ARH (red) colocalizes (yellow) with the dynactin complex protein $p150^{glued}$ (green) at the nuclear envelope. During prometaphase ARH colocalizes with dynein IC (DIC; B) and with a centromere marker (C) at the kinetochores. At the onset of metaphase (D) ARH (red) is found on both kinetochores and spindle poles labeled with γ-tubulin (green). During metaphase (E) ARH colocalizes with γ-tubulin at spindle poles but at the end of anaphase/beginning of telophase (F), ARH is not detectable at the spindle poles labeled with γ-tubulin (arrowheads). During cytokinesis (G and H), ARH and dynein IC (DIC) are found at the midbody. Rat-1 cells (A–F) or HeLa cells (G and H) were fixed with methanol followed by acetone, stained with ARH, markers for the mitotic apparatus or midbody, and DAPI (blue) to detect chromosomes. Bar, 6.5 μm.

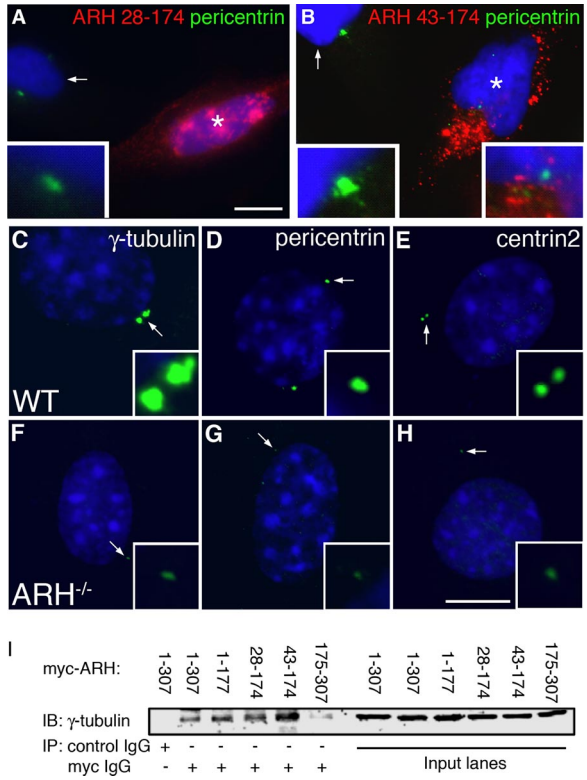


**Figure 8.** Cells expressing C-terminally truncated forms of ARH and $Arh^{-/-}$ MEFs show defects in centrosome assembly. (A and B) HeLa cells expressing myc-$ARH_{28-174}$ or myc-$ARH_{43-174}$ (noncentrosomal targeted forms of ARH). The transfected cell in A (star) has no visible centrosome and the transfected cell in B (star) contains a small centrosome which is enlarged in the right inset. The left insets in each field show a higher magnification of a centrosome from an untransfected cell in the same field (arrows). HeLa cells were transfected with the indicated noncentrosomal targeted forms of ARH and processed for IF. (C–H) $Arh^{-/-}$ MEFs (F–H) have much smaller centrosomes than wt MEFs (C–E) after staining for three centrosome markers: γ-tubulin, pericentrin, or centrin2. MEFs were fixed with −20°C methanol and stained for the indicated centrosome markers (green) and DAPI (blue). Statistical analyses for centrosome size and staining is given in Table 1. (I) γ-Tubulin coimmunoprecipitates with full-length myc-$ARH_{1-307}$ and myc-$ARH_{1-177}$ as well as with myc-$ARH_{28-174}$ and myc-$ARH_{43-174}$ but not with $ARH_{175-307}$. A control mAb was unable to coimmunoprecipitate γ-tubulin from HeLa cells transfected with full-length myc-ARH. HeLa cells were transfected with the indicated constructs and immunoprecipitation was carried out on cell lysates with anti-myc or control IgG.

formation of binucleate cells. These early cytokinesis defects were 60% higher in $Arh^{-/-}$ MEF cells (Video 5) than in their wt counterparts.

## DISCUSSION

Here we report the novel observation that the endocytic adaptor protein ARH localizes in a cell cycle–dependent manner to centrosomes and components of the mitotic apparatus and forms a complex with the motor protein dynein and the γ-tubulin ring complex proteins (γ-TuRC), which are key components of the centrosome. Moreover, the lack of ARH results in smaller or absent centrosomes, a slower growth rate, and prolonged and/or defective cytokinesis. ARH is best known for its role as an endocytic coat protein that selectively facilitates internalization of members of the LDLR superfamily including megalin (Nagai *et al.*, 2003) and LRP and LDLR (Garcia *et al.*, 2001; He *et al.*, 2002; Wilund *et al.*, 2002; Cohen *et al.*, 2003). Thus the presence ARH on centrosomes and the mitotic apparatus raises intriguing questions regarding how it is targeted to these sites and its functions in these locations.

### *ARH Is a Centrosomal Protein*

At interphase a pool of ARH is localized at the centrosome as documented by IF in a number of cell lines and verified with three different ARH antibodies and three different centrosome markers: γ-tubulin, pericentrin, and dynein IC. When myc-tagged rat ARH was expressed in HeLa cells, it also localized to centrosomes. The presence of ARH at centrosomes was further substantiated by cofractionation of ARH with γ-tubulin in centrosome-enriched fractions. Moreover, the centrosomal localization of ARH persisted

**Table 1.** Measurements of centrosome size and staining in wt and $Arh^{-/-}$ MEFs by epifluorescence microscopy and confocal 3D rendering

| | WT MEFs | $Arh^{-/-}$ MEFs |
|---|---|---|
| Epifluorescent microscopic measurements | | |
| Number of cells counted | 54 | 61 |
| Total number of centrosomes counted | 138 | 99 |
| Mean no. of centrosomes/cell | 2.56 ± 0.23 | 1.62 ± 0.16 |
| Mean "area" of each centrosome ($\mu m^2$) | 0.77 ± 0.03 | 0.42 ± 0.02[a] |
| Mean fluorescence intensity of γ-tubulin (per pixel)[a] | 101.9 ± 3.1 | 76.53 ± 3.8[a] |
| Mean integrated fluorescence intensity/centrosome[b] | 8050 ± 459 | 3516 ± 259 |
| Mean centrosomal area/cell ($\mu m^2$)[c] | 2.07 | 0.78 |
| Confocal 3D rendering measurements | | |
| Number of cells counted | 20 | 22 |
| Total number of centrosomes counted | 50 | 44 |
| Mean no. of centrosomes per cell | 2.5 ± 0.25 | 2.0 ± 0.19 |
| Mean volume of each centrosome ($\mu m^3$) | 2 ± 0.17 | 0.88 ± 0.12 |
| Mean centrosomal volume/cell ($\mu m^3$)[d] | 5 ± 0.78 | 1.8 ± 0.27 |

Data represented as mean ± SE.

[a] Average pixel intensity of γ-tubulin staining at each centrosome (per pixel, scale 0–255).

[b] Mean area of centrosome × mean fluorescence intensity of γ-tubulin staining.

[c] Mean number of centrosomes per cell × mean area of cach centrosome.

[d] Mean number of centrosomes per cell × mean volume of each centrosome.

* In ~25% of the $Arh^{-/-}$ MEFs, there was no visible centrosome, and these cells were not included in determining the centrosome area. Hence the reduction in centrosome assembly is more dramatic than is apparent in the "Mean area of each centrosome" and "Mean fluorescence intensity of γ-tubulin at each centrosome." The "Mean centrosomal area/cell," which takes into account both the mean number of centrosome/cell, and the area of each centrosome is a more accurate reflection of the effect of ARH knockout on centrosome assembly.

after disruption of microtubules by nocodazole treatment, indicating ARH is a bona fide centrosomal protein, not a microtubule-associated protein. By mass spectrometry ARH was found to be in a complex with dynein HC and IC, γ-tubulin (GCP1), GCP2, and GCP3, all of which are centrosome (pericentriolar matrix) proteins. Previously we and others have not detected ARH on centrosomes by IF. We believe that most likely this is due to the fact that the more routinely used paraformaldehyde fixation is not optimal for centrosomes.

By truncation analysis we determined that ARH is targeted to centrosomes by its N-terminus (aa 1–177). This region is occupied by the PTB domain and 43 highly conserved N-terminal residues of unknown function. Thus the clathrin and AP-2–binding regions at the C-terminus of ARH are not required for centrosome targeting. Numb is the only other PTB domain protein reported to localize to the centrosome region, which happens during asymmetric cell divisions in the developing *Drosophila* nervous system (Knoblich *et al.*, 1995).

### *ARH Participates in Centrosome Assembly*

Centrosomes are dynamic organelles that are formed and maintained by recruitment of centrosomal proteins from the cytoplasmic pool. They continuously exchange proteins with the cytoplasm, and the sequential assembly of specific proteins at the centrosome is crucial for their numerous functions (Doxsey, 2001). It has been shown that transport and assembly of γ-tubulin and pericentrin onto centrosomes is mediated by dynein (Young *et al.*, 2000; Zimmerman and Doxsey, 2000). Our findings that expression of dominant negative forms of ARH or ARH knockdown (siRNA or $Arh^{-/-}$ MEFs) resulted in smaller or completely absent centrosomes and reduced staining of the centrosome markers γ-tubulin, pericentrin, and centrin2 at the centrosome strongly suggest that ARH is involved in centrosome assembly, likely through a dynein-dependent mechanism.

### *The Localization of ARH Is Regulated in a Cell Cycle–dependent Manner*

We found that ARH resembles dynein and to a certain extent dynactin and γ-tubulin in its localization and behavior during the cell cycle: Both dynein and ARH associate with centrosomes during interphase and localize sequentially to the nuclear envelope, kinetochores, and spindle poles during mitosis and to the midbody during cytokinesis (Quintyne and Schroer, 2002; Salina *et al.*, 2002; reviewed in Karki and Holzbaur, 1999). Dynein is a minus-end motor that has important functions during both interphase and mitosis. During interphase it functions in the trafficking of protein complexes (e.g., γ-tubulin, pericentrin) and membrane vesicles along microtubules (Schroer, 2004) and participates in centrosome assembly (Young *et al.*, 2000). During mitosis it functions in nuclear membrane breakdown, spindle checkpoint inactivation, spindle positioning, separation of daughter centrosomes, and cytokinesis (Howell *et al.*, 2001; Salina *et al.*, 2002; Delcros *et al.*, 2006; reviewed in Karki and Holzbaur, 1999). The presence of dyneins on a pool of vesicles immunoisolated with ARH is in keeping with the previous finding of dynein on vesicles with aquaporin-2 (Marples *et al.*, 1998) and suggests that trafficking of ARH-bearing vesicles from the PM to pericentriolar-recycling endosomes involves cytoplasmic dynein as a molecular motor. Based on our finding that ARH and dynein have similar cell cycle–dependent localizations and that ARH resembles dynein in its dynamic behavior, it is tempting to speculate that ARH participates in some of dynein's functions during interphase and mitosis.

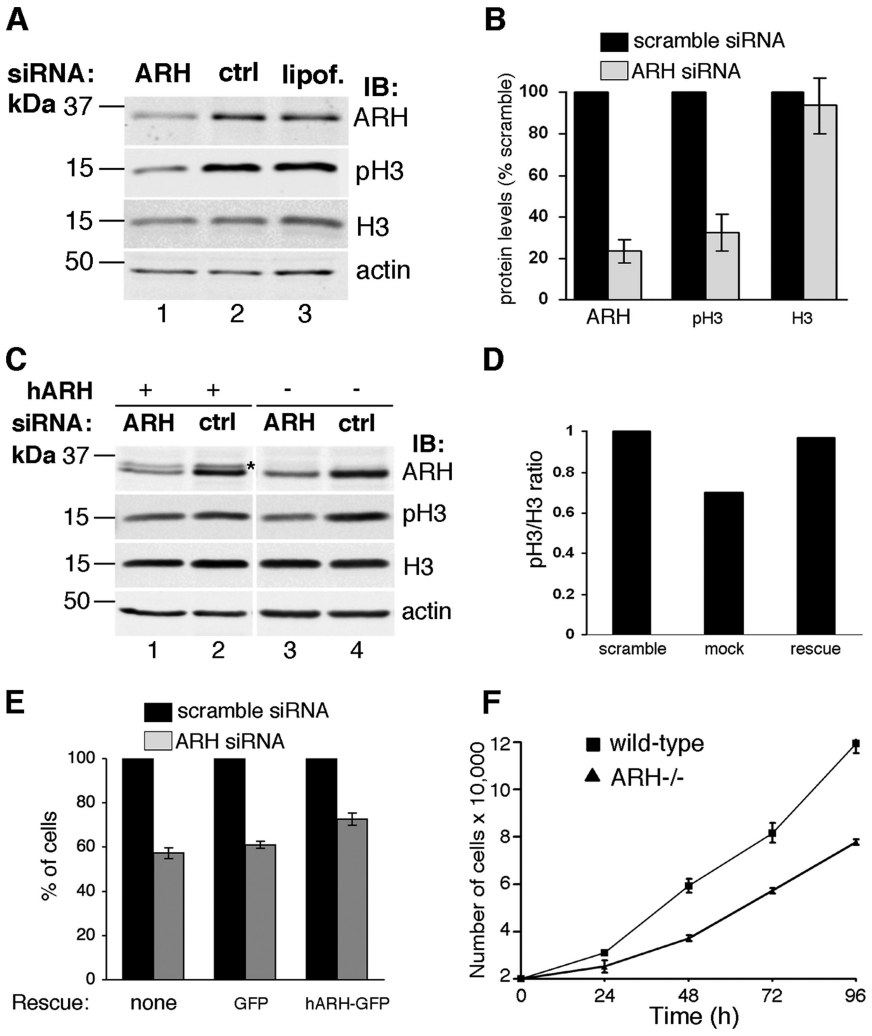


**Figure 9.** ARH depletion affects cell cycle progression. (A) Phosphohistone-H3 (pH3), a mitosis marker, is reduced by 55–85% in ARH-depleted cells (lane 1), indicating reduced entry into mitosis. Total histone-H3 (H3) is not significantly changed. ARH siRNA leads to a 69–87% reduction in ARH. Rat-1 cells were transfected with rat ARH smartpool siRNA (ARH), scramble siRNA (ctrl), or Lipofectamine 2000 alone (lipof.) and analyzed 48 h after transfection. (B) Quantification of protein levels of three replicate blots as in A. The levels of ARH, phosphohistone-H3(pH3), and total histone (H3) are expressed as % of the scramble control (set to 100%). (C) Phosphohistone-H3 levels are partially restored upon introduction of full-length human ARH into ARH siRNA-treated cells (lane 1). The band for human ARH (asterisk, lane 2) appears weak due to the fact that the ARH antibody was made against rat ARH and reacts only weakly with transfected human ARH. Retroviral infection with hARH was performed 15 h after siRNA transfection followed by analysis 48 h later. (D) Quantification of levels of phosphohistone H3 (pH3) and total histone H3 (H3) after infection of ARH siRNA-treated cells with a control (mock) or hARH virus (rescue). The data represent the mean of three replicate analyses as in C. The levels are expressed as a ratio of pH3/H3, with the mean of the ratio of the scramble control set to 1. (E) Bar graph showing effects of ARH depletion on cell growth. Rat ARH siRNA-treated cells grow more slowly than controls treated with scramble siRNA. This effect is partially rescued by expressing full-length human ARH-GFP (hARH-GFP) in siRNA-treated cells, whereas expression of GFP alone has no significant effect. Retroviral infection (hARH) was performed 24 h after siRNA transfection, and the number of cells/well were counted 48 h later. (F) wt and $Arh^{-/-}$ MEF cell numbers were counted at the indicated times after plating. $Arh^{-/-}$ MEFs grow more slowly than wt cells.

### *Involvement of ARH in Mitosis/Cytokinesis*

From a functional standpoint, centrosomes nucleate microtubules and also regulate multiple steps in the cell cycle, i.e., regulation of G1/S transition, formation of spindle poles, metaphase–anaphase transition, and cytokinesis (Piel *et al.*, 2001; Doxsey *et al.*, 2005). Consistent with a role for ARH in centrosome functions, ARH-depleted cells showed reduced phosphorylation of histone H3, indicative of reduced entry into mitosis, most likely due to a cell cycle arrest/delay caused by aberrant centrosome assembly. Similarly, both ARH siRNA-treated cells and $Arh^{-/-}$ MEFs showed a reduced growth rate and a significant delay in the completion of cytokinesis compared with wt cells. Cells depleted of ARH remained interconnected with long cytoplasmic bridges for extended periods indicative of a defect in the terminal scission step in cytokinesis. The requirement for a functional centrosome as well as the role of a number of centrosome components in cytokinesis has been well documented (Piel, 2001; Doxsey *et al.*, 2005). For example, a similar inability of cells to complete cytokinesis has been reported in cells from which the centrosome has been removed (Hinchcliffe *et al.*, 2001; Khodjakov and Rieder, 2001; Piel, 2001). Thus the lack of ARH leading to small or absent centrosomes could similarly lead to defects in cytokinesis and progression of the cell cycle.

### *Endosomal Proteins in Centrosomal and Mitotic Functions*

An increasing number of proteins that are traditionally endocytic proteins or have been localized to endocytic compartments have also been reported to be present at the centrosome, the mitotic spindle, or the midbody. Dynamin-2, a GTPase known mainly for its role in pinching off vesicles from the cytoplasmic face of membrane compartments, has been reported to mediate centrosome cohesion (i.e., negative regulation of centrosome separation; Thompson *et al.*, 2004) and to localize to the midbody where it is required for completion of cytokinesis. Similarly, clathrin heavy chain has been localized to both the mitotic spindle where it is required for chromosome separation (Royle *et al.*, 2005) and to the midbody where it is required for completion of cytokinesis (Niswonger and O'Halloran, 1997; Konopka *et al.*, 2006). Finally, the endocytic adaptor RLIP76, an effector of the Ral GTPase family, was reported to localize to centrosomes where it facilitates their separation and movement to the mitotic poles (Rosse *et al.*, 2003).

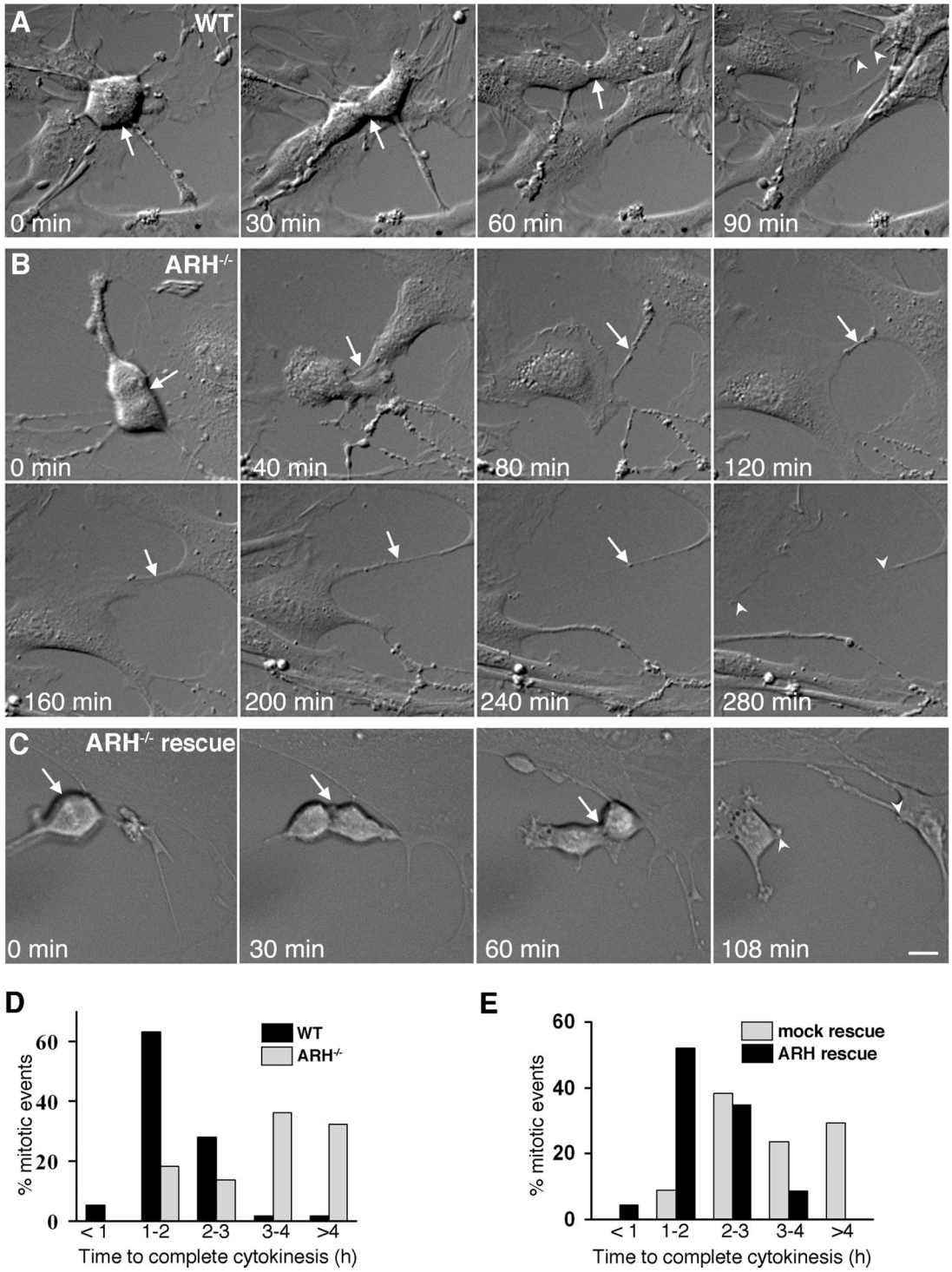


**Figure 10.** $Arh^{-/-}$ MEFs show a delay in cytokinesis and have increased numbers of binucleate cells. (A–C) Differential interference contrast images of typical mitotic events in wt MEFs (A), $Arh^{-/-}$ MEFs (B), and $Arh^{-/-}$ MEFs infected with pMSCV-ARH (rescue; C) obtained by time-lapse microscopy at the indicated time points. The cleavage furrow and cytokinesis bridge are indicated by arrows. Arrowheads in the last frame of each panel indicate the completely separated daughter cells. Videos of these mitotic events as well as additional examples are available as Online Supplemental Material. Bar, 12 $\mu$m. (D) Frequency distribution of the time taken by wt and $Arh^{-/-}$ MEF cells to complete cytokinesis. For wt MEFs, n = 57 and for $Arh^{-/-}$ MEFs, n = 44. (E) Frequency distribution of the time taken by $Arh^{-/-}$ MEFs to complete cytokinesis after either mock infection or infection (mock rescue) with pMSCV-ARH virus (ARH rescue). For mock infection, n = 34 and for pMSCV-ARH infection, n = 23.

ARH marks yet another example of the connection between endocytosis and mitosis. ARH can bind to the cytoplasmic tail of LDLR family members and to membranes via phosphoinositides (Garcia *et al.*, 2001; He *et al.*, 2002; Mishra

*et al.*, 2002, 2005) as well as to centrosomes where it affects centrosome assembly. What is the possible mechanism by which this endocytic protein is involved in centrosome assembly? Although there is a large pool of γ-tubulin in the cytosol (Moudjou *et al.*, 1996), we and others (Dryková *et al.*, 2003, Efimov *et al.*, 2007) have found γ-tubulin in membrane fractions/complexes as well. ARH appears to interact with both the cytosolic as well as the membrane pools of γ-tubulin and dynein, and a pool of γ-TuRC proteins and dynein are found on vesicles immunoisolated with ARH, in keeping with the previous finding of dynein on vesicles with aquaporin-2 (Marples *et al.*, 1998). These findings raise the intriguing possibility that ARH could be involved in trafficking γ-tubulin along a vesicular pathway driven by the dynein motor. Thus the role of ARH in centrosome assembly could represent an extension of its membrane trafficking function. Indeed we have previously shown that ARH accompanies megalin along its endocytic route to pericentriolar recycling endosomes. Our electron microscopic studies indicate that vesicles bearing ARH dock at the periphery of endosomes (Nagai *et al.*, 2003), which is consistent with the idea that ARH could be involved in trafficking centrosome components via a vesicular pathway for delivery to the pericentriolar matrix. Trafficking of ARH to the centrosome may in turn also serve as a signal for the regulation of centrosome functions in response to endocytic stimuli. Thus ARH may be part of the machinery involved in synchronizing endocytic, centrosomal, and mitotic functions.

## ACKNOWLEDGMENTS

We thank Dr. Joachim Herz (University of Texas Southwestern, Dallas, TX) for generously providing the wild-type and $Arh^{-/-}$ MEFs. Time-lapse and confocal imaging studies were carried out at the UCSD Neuroscience Microscopy Shared Facility (National Institute of Neurological Disorders and Stroke Grant P30 NS047101). This work was supported by National Institutes of Health Grant DK17724 (M.G.F.). S.L. was supported in part by the Academy of Finland, Sigrid Juselius Foundation, and Finnish Cultural Foundation and R.N. by the Carlsberg Foundation.

## REFERENCES

Blomberg-Wirschell, M., and Doxsey, S. J. (1998). Rapid isolation of centrosomes. Methods Enzymol. *298*, 228–238.

Bornens, M., Paintrand, M., Berges, J., Marty, M. C., and Karsenti, E. (1987). Structural and chemical characterization of isolated centrosomes. Cell Motil. Cytoskelet. *8*, 238–249.

Brett, T. J., and Traub, L. M. (2006). Molecular structures of coat and coat-associated proteins: function follows form. Curr. Opin. Cell Biol. *18*, 395–406.

Cohen, J. C., Kimmel, M., Polanski, A., and Hobbs, H. H. (2003). Molecular mechanisms of autosomal recessive hypercholesterolemia Curr. Opin. Lipidol. *14*, 121–127.

Delcros, J. G., Prigent, C., and Giet, R. (2006). Dynactin targets Pavarotti-KLP to the central spindle during anaphase and facilitates cytokinesis in *Drosophila* S2 cells. J. Cell Sci. *119*, 4431–4441.

Doxsey, S., McCollum, D., and Theurkauf, W. (2005). Centrosomes in cellular regulation. Annu. Rev. Cell Dev. Biol. *21*, 411–434.

Doxsey, S. (2001). Re-evaluating centrosome function. Nat. Rev. Mol. Cell Biol. *2*(9), 688–698.

Dryková, D., Cenklová, V., Sulimenko, V., Volc, J., Dráber, P., and Binarová, P. (2003). Plant gamma-tubulin interacts with alphabeta-tubulin dimers and forms membrane-associated complexes. Plant Cell *15*(2), 465–480.

Efimov, A. *et al.* (2007). Asymmetric CLASP-dependent nucleation of noncentrosomal microtubules at the trans-Golgi network. Dev. Cell *12*(6), 917–930.

Garcia, C. K. *et al.* (2001). Autosomal recessive hypercholesterolemia caused by mutations in a putative LDL receptor adaptor protein. Science *292*, 1394–1398.

Gotthardt, M., Trommsdorff, M., Nevitt, M. F., Shelton, J., Richardson, J. A., Stockinger, W., Nimpf, J., and Herz, J. (2000). Interactions of the low density lipoprotein receptor gene family with cytosolic adaptor and scaffold proteins suggest diverse biological functions in cellular communication and signal transduction. J. Biol. Chem. *275*, 25616–25624.

He, G., Gupta, S., Yi, M., Michaely, P., Hobbs, H. H., and Cohen, J. C. (2002). ARH is a modular adaptor protein that interacts with the LDL receptor, clathrin, and AP-2. J. Biol. Chem. *277*, 44044–44049.

Hinchcliffe, E. H., Miller, F. J., Cham, M., Khodjakov, A., and Sluder, G. (2001). Requirement of a centrosomal activity for cell cycle progression through G1 into S phase. Science *291*, 1547–1550.

Howell, B. J., McEwen, B. F., Canman, J. C., Hoffman, D. B., Farrar, E. M., Rieder, C. L., and Salman, E. D. (2001). Cytoplasmic dynein/dynactin drives kinetochore protein transport to the spindle poles and has a role in mitotic spindle checkpoint inactivation. J. Cell Biol. *155*, 1159–1172.

Jones, C., Hammer, R. E., Li, W. P., Cohen, J. C., Hobbs, H. H., and Herz, J. (2003). Normal sorting but defective endocytosis of the low density lipoprotein receptor in mice with autosomal recessive hypercholesterolemia. J. Biol. Chem. *278*, 29024–29030.

Karki, S., and Holzbaur, E.L.F. (1999). Cytoplasmic dynein and dynactin in cell division and intracellular transport. Curr. Opin. Cell Biol. *11*, 45–53.

Keyel, P. A., Mishra, S. K., Roth, R., Heuser, J. E., Watkins, S. C., and Traub, L. M. (2006). A single common portal for clathrin-mediated endocytosis of distinct cargo governed by cargo-selective adaptors. Mol. Biol. Cell *17*, 4300–4317.

Khodjakov, A., and Rieder, C. L. (2001). Centrosomes enhance the fidelity of cytokinesis in vertebrates and are required for cell cycle progression. J. Cell Biol. *153*, 237–242.

Knoblich, J. A., Jan, L. Y., and Jan, Y. N. (1995). Asymmetric segregation of Numb and Prospero during cell division. Nature *377*, 624–627.

Konopka, C. A., Schleede, J. B., Skop, A. R., and Bednarek, S. Y. (2006). Dynamin and cytokinesis. Traffic *7*(3), 239–47.

Lehtonen, S., Lehtonen, E., Kudlicka, K., Holthöfer, H., and Farquhar, M. G. (2004) Nephrin forms a complex with adherens junction proteins and CASK in podocytes and in Madin-Darby canine kidney cells expressing nephrin. Am. J. Pathol. *165*(3), 923–936.

Marples, D., Schroer, T. A., Ahrens, N., Taylor, A., Knepper, M. A., and Nielsen, S. (1998). Dynein and dynactin colocalize with AQP2 water channels in intracellular vesicles from kidney collecting duct. Am. J. Physiol. *274*, F384–F394.

Maurer, M. E., and Cooper, J. A. (2006). The adaptor protein Dab2 sorts LDL receptors into coated pits independently of AP-2 and ARH. J. Cell Sci. *119*, 4235–4246.

Mishra, S. K., Watkins, S. C., and Traub, L. M. (2002). The autosomal recessive hypercholesterolemia (ARH) protein interfaces directly with the clathrin-coat machinery. Proc. Natl. Acad. Sci. USA *99*, 16099–16104.

Mishra, S. K., Keyel, P. A., Edeling, M. A., Dupin, A. L., Owen, D. J., and Traub, L. M. (2005). Functional dissection of an AP-2 beta2 appendage-binding sequence within the autosomal recessive hypercholesterolemia protein. J. Biol. Chem. *280*, 19270–19280.

Mitchison, T. J., and Kirschner, M. W. (1986). Isolation of mammalian centrosomes. Methods Enzymol. *134*, 261–268.

Moritz, M., and Agard, D. A. (2001). Gamma-tubulin complexes and microtubule nucleation. Curr. Opin. Struct. Biol. *11*, 174–181.

Moudjou, M., Bordes, N., Paintrand, M., and Bornens, M. (1996). Gamma-tubulin in mammalian cells: the centrosomal and the cytosolic forms. J. Cell Sci. *109*, 875–887.

Nagai, M., Meerloo, T., Takeda, T., and Farquhar, M. G. (2003). The adaptor protein ARH escorts megalin to and through endosomes. Mol. Biol. Cell *14*, 4984–4996.

Niswonger, M. L., and O'Halloran, T. J. (1997). A novel role for clathrin in cytokinesis. Proc. Natl. Acad. Sci. USA *94*, 8575–8578.

Piel, M., Nordberg, J., Euteneuer, U., and Bornens, M. (2001). Centrosome-dependent exit of cytokinesis in animal cells. Science *291*, 1550–1553.

Quintyne, N. J., and Schroer, T. A. (2002). Distinct cell cycle-dependent roles for dynactin and dynein at centrosomes. J. Cell Biol. *159*, 245–254.

Rosse, C., L'Hoste, S., Offner, N., Picard, A., and Camonis, J. (2003). RLIP, an effector of the Ral GTPases, is a platform for Cdk1 to phosphorylate epsin during the switch off of endocytosis in mitosis. J. Biol. Chem. *278*, 30597–30604.

Royle, S. J., Bright, N. A., and Lagnado, L. (2005). Clathrin is required for the function of the mitotic spindle. Nature *434*, 1152–1157.

Salina, D., Bodoor, K., Eckley, D. M., Schroer, T. A., Rattner, J. B., and Burke, B. (2002). Cytoplasmic dynein as a facilitator of nuclear envelope breakdown. Cell *108*, 97–107.

Schiebel, E. (2000). Gamma-tubulin complexes: binding to the centrosome, regulation and microtubule nucleation. Curr. Opin. Cell Biol. *12*, 113–118.

Schroer, T. (2004). Dynactin. Annu. Rev. Cell Dev. Biol. *20*, 759–779.

Stolt, P. C., and Bock, H. H. (2006). Modulation of lipoprotein receptor functions by intracellular adaptor proteins. Cell Signal. 18(10):1560–1571.

Thompson, H. M., Cao, H., Chen, J., Euteneuer, U., and McNiven, M. A. (2004). Dynamin-2 binds gamma-tubulin and participates in centrosome cohesion. Nat. Cell Biol. *6*, 335–342.

Vallee, R. B., Williams, J. C., Varma, D., and Barnhart, L. E. (2004). Dynein: an ancient motor protein involved in multiple modes of transport. J. Neurobiol. *58*, 189–200.

Wilund, K. R., Yi, M., Campagna, F., Arca, M., Zuliani, G., Fellin, R., Ho, Y.-K., Garcia, J. V., Hobbs, H. H., and Cohen, J. C. (2002). Molecular mechanisms of autosomal recessive hypercholesterolemia. Hum. Mol. Genet. *11*, 3019–3030.

Young, A., Dictenberg, J. B., Purohit, A., Tuft, R., and Doxsey, S. J. (2000). Cytoplasmic dynein-mediated assembly of pericentrin and gamma tubulin onto centrosomes. Mol. Biol. Cell *11*, 2047–2056.

Zheng, Y., Wong, M. L., Alberts, B., and Mitchison, T. (1995). Nucleation of microtubule assembly by a gamma-tubulin-containing ring complex. Nature *378*, 578–583.

Zimmerman, W., and Doxsey, S. J. (2000). Construction of centrosomes and spindle poles by molecular motor-driven assembly of protein particles. Traffic. *1*(12), 927–934.

Zhou, W., Ryan, J. J., and Zhou, H. (2004). Global analyses of sumolyated proteins in *Saccharomyces cerevisiae*. J. Biol. Chem. *279*, 32262–32268.